Towards Establishing a Vertical Distribution of NO_2 and NO_3 in a Night-Time Urban Environment

William Fujs

Supervisor:

Dr. McLaren

Committee:

Dr. Harris

Dr. Rudolph

Course Director:

Dr. Wilson

Abstract

Atmospheric NO_2 and NO_3 are investigated using Active-Differential Optical Absorption Spectroscopy (DOAS). A data set for the concentrations of these species was created using night-time observations between March 4 - 8 and March 23 – 26, 2015. Comparisons between the DOAS results were made with a TECO instrument to validate the methodology for fitting both species. NO_2 and NO_3 were fit in the wavelength ranges of 560-585nm and 617-670nm, respectively. Atmospheric stability has been shown to be an indicator for the presence of NO_3. Two case studies are presented to highlight the difference in night-time chemistry under different atmospheric conditions. March 5, 2015 is used to display the results of stable night and March 8, 2015 is used to represent an unstable night. With the confirmation of the methodology used to fit both NO_2 and NO_3 simultaneously a vertical distribution will be able to established using these techniques. This will be accomplished by collecting data over the course of a night at two angles and combining it with a Lunar DOAS data.

Acknowledgements

I would first like to thank Dr. McLaren for his guidance throughout this project. My work would not have been possible without his constant direction and leadership during this process. I would also like to thank the members of the McLaren research group, firstly Zoe Davis for her help throughout this project. Her ongoing feedback and support ensured that I was always on track. I would also like to thank Kevin Nikelski for his help in the starting of my project. I would also like to thank Dr. Rudolph and Dr. Harris for being on my thesis committee.

I would also like to thank the Center for Atmospheric Chemistry at York University which allowed my research project to occur. Special thanks to Carol Weldon for her support and handling of administrative duties, making sure that everything runs smoothly.

Table of Contents

1. Introduction

1.1 Overview of the Atmosphere

All life on the planet is sustained, at least in part, by the atmosphere. Understanding changes in the atmosphere can be achieved by gaining a deeper insight into the current composition and distribution of the particles in the atmosphere. The atmosphere extends over the planet to a height of roughly 100 km, the Karman line, above which it thins considerably. [1] The vertical distribution of this distance is broken up into different regions based on the particles present and temperatures. The order of these regions, in ascending order is; troposphere, stratosphere, mesosphere and thermosphere. During the daytime sunlight warms the surface causing air to rise and expand which in turn cools the air. This vertical mixing will play an important within the lower portion of the troposphere and the observed atmospheric chemistry.

Within each of the atmospheric regions, sub-regions exist. Of particular interest is the lower 0.5-2 km of the troposphere which is referred to as the boundary layer. This portion of the troposphere undergoes a well established cycle of mixing between sunrise and sunset, see Figure 1.1.

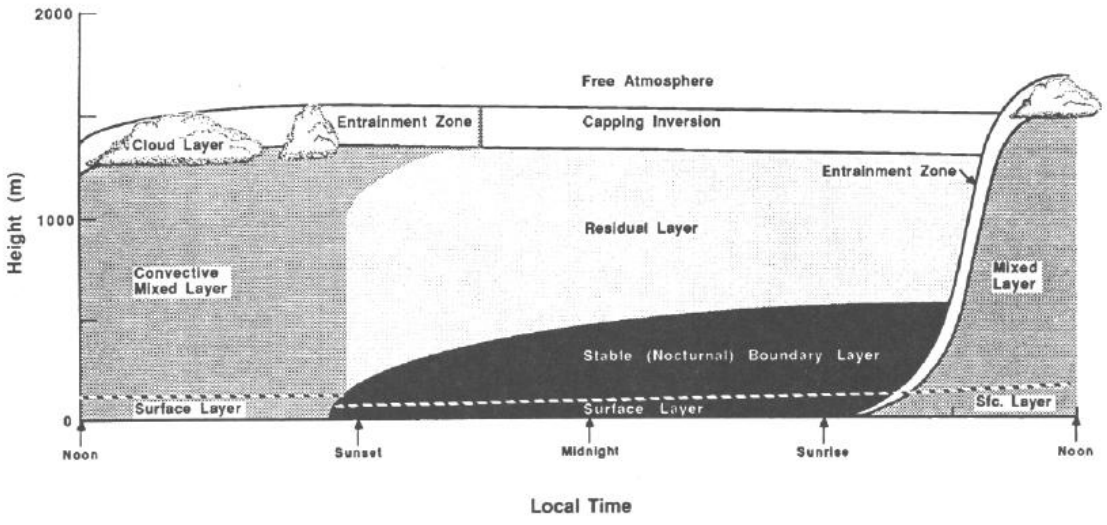

Figure 1.1: The vertical mixing of air masses from day to night and the development of the stable nocturnal boundary layer. Taken from Stull 1988.

During the night time the lower portion of the boundary layer undergoes cooling releasing heat and forms the Nocturnal Boundary Layer (NBL). Above the NBL is the Residual Layer (RL), effectively an air mass composed of the previous day's particles. After sunrise the NBL will be heated and expand mixing with the RL to form the stable Convection Mixed Layer (CML) during the day. The mixing of these air masses is of interest as gases from one night will directly affect the atmosphere the following day.

1.2 Nitrogen Atmospheric Chemistry

Only four gases make up 99.99% of the total atmosphere; N_2, O_2, Ar and CO_2 excluding water [2] Despite the low abundance of the trace gases they play a major role in atmospheric chemistry and climate. Many interactions between gases have been shown to occur. Nitrogen oxide compounds in the atmosphere are commonly referred to as NO_x (= NO + NO_2) The major source of NO_x is anthropogenic combustion of substances containing N_2 gas which reacts, in high temperatures, with O_2 to form either NO or NO_2. The ratio of NO to NO_2 produced is dependent on a variety of factors including fuel and type of combustion. [2] NO_2 can then undergo photolysis when exposed to wavelengths of light below 420nm through the following reaction;

$$NO_2 + h\nu \rightarrow NO + O(\,^3P) \qquad \text{(R. 1)}$$

The triplet state oxygen that is formed will rapidly react with neighbouring atmospheric O_2 in the following way to produce ozone;

$$O(\,^3P) + O_2 \rightarrow O_3 \qquad \text{(R. 2)}$$

Any NO in the atmosphere, produced from the initial NO_2 photolysis will quickly react with this newly formed O_3 through the reaction;

$$NO + O_3 \rightarrow NO_2 + O_2 \qquad \text{(R. 3)}$$

This set of reaction dictates that there is a constant exchange taking place between the amount of O_3 and NO_2 present in the atmosphere. In an environment with high levels of NO it is expected that O_3 concentrations will be reduced to levels below detection limits. This is

especially true during the night where new O_3 is not readily added to the atmosphere as a result of NO_2 photolysis being absent.

The nitrate radical, normally present at appreciable levels only at night, also undergoes photolysis during the daytime and can react through one of two possible reactions; [7]

$$NO_3 + hv \rightarrow NO + O_2 \quad \text{(R. 4)}$$

$$NO_3 + hv \rightarrow NO_2 + O \quad \text{(R. 5)}$$

Formation of NO_3 has been shown to occur through the following reaction;

$$NO_2 + O_3 \rightarrow NO_3 + O_2 \quad \text{(R. 6)}$$

When NO_x concentrations are at significantly high concentrations NO_3 will be removed from the atmosphere through the following reaction;

$$NO_3 + NO \rightarrow 2NO_2 \quad \text{(R. 7)}$$

However, this reaction can be impeded if there is a significant amount of O_3 present at the same time as NO;

$$NO + O_3 \rightarrow NO_2 + O_2 \quad \text{(R. 8)}$$

This reaction acts as a predictor for NO_3 being present at detectable levels. If there is NO present it is expected that there will not be any NO_3. It has been shown that the ideal conditions for detecting NO_3 in the urban atmosphere are on a windy night (WS > 2 m/s) with $\Delta T_{9.5m\text{-}1.0m} \leq 0.2^oC$. [8] These conditions will lead to vertical mixing resulting in NO_3 not being removed from the atmosphere through either of the above reactions.

If concentrations of NO_3 are present at high enough concentrations the nitrate radical can react with atmospheric NO_2 through the following reaction;

$$NO_3 + NO_2 \rightleftharpoons N_2O_5 \quad \text{(R. 9)}$$

The dinitrogen pentoxide molecule is of particular interest as its concentration cannot currently be directly studied. The process of finding the concentrations of NO_3 and NO_2 will allow accurate approximations of N_2O_5 to occur using the equilibrium constant of this reaction. [9]

$$[N_2O_5] \rightleftharpoons k[NO_3][NO_2] \quad \text{(R. 10)}$$

1.3 Differential Optical Spectroscopy

In order to probe the atmosphere for these substances a spectroscopic technique known as DOAS (Differential Optical Absorption Spectroscopy) is employed. This technique is able to quantify the concentration of a wide array of gas species through analysis of the absorbed wavelengths of light. This is accomplished by characterizing the difference in emitted light with what is detected. By identifying cross-sections of known gases to the collected spectrum their concentrations can be quantified. Since DOAS was demonstrated to be able to make measurements of trace gases by Platt et. al. in 1979 [3], DOAS has been used to also identify a variety of other atmospheric gases including OH (Perner et. al. 1976), HONO (Perner and Platt 1979), NO_3 (Platt and Perner 1980), BrO (Saunder et. al. 1989), IO (Alicke 1999) and CHOCHO (Volkamer et. al. 2005) and others

There are two major groups that DOAS techniques can fall into; either active or passive. Passive-DOAS techniques rely on a naturally occurring light source, most commonly the moon or sun, with a few reports of stars being used. Passive techniques allow for the application of the Beer-Lambert law which most spectroscopic techniques follow. This technique allows for the concentration along the path of light to be calculated. Through the use of transformative geometric calculations a vertical column density (VCD) is then able to be calculated.

Conversely, Active-DOAS relies on an artificial light source to probe the atmosphere. This technique is able to detect low concentrations (ppt) due to the long path length that is used. As space is often a challenge many different Active-DOAS light-path arrangements exist all of which act to provide the longest path length possible. This set of experiments will employ a retro reflector to reflect the signal back to the light source to be detected.

1.4 DOAS Theory

The goal of DOAS techniques is to determine the concentration of a particular gas present in the atmosphere. This is complicated by multiple factors that attenuate the light as it travels along the light path from the light source to the instrument. The effects of Rayleigh and Mie scattering and aerosol extinction, turbulence and trace gases affect the spectrum produced with broad band features. The DOAS technique solves these complications by finding a way to not need to quantify these factors but separating out the features we use to identify gases of interest. Molecules of interest to atmospheric chemistry often present very sharp narrow-band spectrum, differential features. [3] The goal of the DOAS process is then to separate the broad band features from the narrow band features in a spectrum which was collected probing the atmosphere. This is accomplished by fitting a polynomial to a spectrum to account for the broadband features and separating out the narrow band features due to absorption by trace gases present.

$$I(\lambda) = I_o(\lambda)e^{(-\sigma(\lambda)Lc)}$$

(E. 1)

I$o(\lambda)$ represents the initial light intensity emitted by the lamp, while I_o is the final light intensity. The concentration of the absorber, c, typically has units of molecules/cm, over the path length, L, which has units of cm. The absorption cross-section is represented by $\sigma(\lambda)$. The amount that the light is affected by a medium it passes through is referred to as Optical density which can be calculated using equation

$$D = \ln\frac{I_o(\lambda)}{I(\lambda)} = \sigma(\lambda)Lc$$

(E. 2)

The concentration of a particular absorber can be determined using equation #.

$$c = \ln\frac{I_o(\lambda)}{I(\lambda)}\frac{1}{\sigma(\lambda)} = \frac{D}{\sigma(\lambda)L} \qquad \text{(E. 3)}$$

In order to quantify the concentration of a gas in the atmosphere without separating out its narrow band features, you would have to account for all other factors that attenuate the light in the atmosphere, including Mie and Rayleigh scattering. Take all atmospheric factors into account Rayleigh scatting must all be added to the calculations. This is the scattering of light as it passes through particles in the air.

$$\epsilon_R(\lambda) = \sigma_R(\lambda) n_{air} \quad (E.4) \qquad \sigma_R(\lambda) = \sigma_{RO}\lambda^{-4} \quad (E.5)$$

Where $n_{air} = 2.45 \times 10^{19}$ molecules/cm under standard conditions (P=1 atm, T=298 K) and $\sigma_{RO} = 4.4 \times 10^{-16}$ cm^2nm^4. Another factor to include into these calculations is Mie extinction which refers to the light scattering as aerosol particles with dimensions approaching the same order of λ as light it interacts with.

$$\epsilon_M(\lambda) = \epsilon_{MO}\lambda^{-4} \quad \text{(E. 6)}$$

When the Mie extinction and Rayleigh scattering are applied to the Beer-Lambert law the equation becomes

$$I(\lambda) = I_o(\lambda) e^{(-\sigma(\lambda)Lc + \epsilon_R(\lambda) + \epsilon_M(\lambda))} \quad \text{(E. 7)}$$

The differential optical density $\tau'(\lambda, T)$ is represented as;

$$\tau'(\lambda, T) = \ln\left(\frac{I_0'(\lambda, L)}{I(\lambda, L)}\right) \quad \text{(E. 8)}$$

The amount of absorber along the slant light path can be expressed as the Slant Column Density (SCD) S;

$$S = \int_0^L c(l) dl \quad \text{(E. 9)}$$

This relation produces a value of S with the units $\frac{molecules}{cm^2}$ as the concentration $c(l)$ is integrated along the path length L. The overall value measured by DOAS can then be found by combining the value of S with differential optical density.

$$S = \frac{\tau'(\lambda,T)}{\sigma'(\lambda,p,T)} \quad \text{(E. 10)}$$

The updated Beer-Lambert equation for the light collected by the DOAS instrument can be expressed as.

$$\ln\left(I(\lambda,L) = \ln\big(I_o(\lambda)\big) - \int_o^L \Big\{\sum_{j=1}^{n}\big[\sigma_j^i(\lambda,p,T) + \sigma_{Bj}(\lambda,p,T)\big] \times c_j(l) + \epsilon_R(\lambda,l) + \epsilon_M(\lambda,l)\Big\}\, dl\right.$$

(E.11)

For an explanation on the DOASIS software package fitting a polynomial to the broadband features of the spectrum please see experimental section 2.3 Polynomial Fitting.

1.5 Towards Determining a Vertical Distribution of NO_2 and NO_3

The long term goal of this project is then to simultaneously determine a vertical distribution of NO_2 and NO_3. This will allow for the calculation of N_2O_5 concentration using equation 1.1. These measurements will be made using two retroreflectors which will be alternated between during the course of a night. This will give the concentrations of these gas species over two horizontal paths with different angles. These values will be combined with measurements being taken using Lunar DOAS on the same nights to establish a total vertical distribution.

2. Experimental

2.1 Data Collection

A modified 2000 Active-DOAS instrument was used to measure nocturnal mixing ratios of NO_3, NO_2, O_4 and H_2O at York University, Keele campus. The instrument light source was a high pressure 150W Xenon arc lamp. The light beam was returned to the instrument detector by a 30 cube retro-reflector for a total light path length of 2.2km.

Figure 2: Google Earth image of York University campus showing the total DOAS light path length

The light was then focused onto a fiber optic cable, which carried the signal to an Ocean Optics S2000 temperature controlled spectrometer with a wavelength range of 550-835nm. The signal was then transferred to a computer that used the OOIBase32 software package to collect the data as a spectrum of intensity with wavelength.

2.2 Spectral Fitting

By combining the offset, dark noise, mercury/neon and lamp spectrum a fitting scenario is created using the DOASIS software. A fitting region is chosen in order to detect the species of interest. This region should include distinct peaks in the cross-section of the gas chosen to fit. The region should also not have any other significant features either from the lamp. A 2nd order polynomial is then used to account for the broadband effects of Rayleigh and Mie scattering.

In order to create a complete fit scenario for each spectrum collected the software DOASIS was used. In order to correct for calibrate instrumental noise dark current and offset spectra must be collected. First, an offset spectrum is taken in order to account for an artificial background electronic signal produced within the spectrometer. This is achieved by removing the fiber from the Active-DOAS and capping the end of the fiber cable to block all incoming light to the spectrometer. The offset spectrum is then collected with an integration time of seven milliseconds and 30000 averages. This spectrum was subtracted from each sample spectrum before any further calibration is done. Due to the electronic offset signal being dependent on temperature the offset spectra were collected before each night's samples were taken. This was done to account for any variance in temperature. The offset spectrum can be represented as;

$$I_{corrected}(n) = I(n) - \frac{n_{meas}}{N_{OS}} \cdot I_{OS}(n) \qquad \text{(E. 12)}$$

Where the signal of pixel n is represented by $I_{corrected}(n)$ and $I(n)$ before and after the correction, respectively. n_{meas} and N_{OS} are the number of scans taken to make the measured and offset spectrum, respectively, and $I_{OS}(n)$ is the offset signal.

A dark noise spectrum must also be subtracted from each spectrum. The dark noise spectrum is collected with an integration time of 10000 millisecond and 15 averages. This spectrum accounts for thermal electrons and associated noise being detected by the spectrometer and is subtracted from each spectrum prior to a fit. This dark noise spectrum must be correct to account for the differences in integration times used to collect it and each sample spectrum. This is achieved by multiplying the dark noise spectrum by a ratio of the

integration time used on the sample and dark spectrum. The dark current spectrum can be represented as follows;

$$I_{corrected}(n) = I(n) - \frac{t_{meas}}{t_{DC}} \cdot I_{DC,corr}(n) \quad \text{(E. 13)}$$

This formula follows a similar pattern to that of the offset where $I_{DC,corr}(n)$ is the signal of pixel n being corrected. This measurement takes into account the affect that varying temperature can have on a signal.

Calibration lines are collected by using two separate light sources one Mercury and another Helium Neon lamp. This spectrum is collected by aiming the light of both lamps on to one spot of a clear white paper and focusing the end of the fiber optic cable on this point while blocking all other external light. These peaks allow for each sample spectrum collected to be corrected for any shift as a result of temperature changes. The measured spectrum is calibration using the known wavelength locations of the measured peaks. The main peaks used in this set of experiments are the Neon peak at 632.8nm and two Mercury peaks at 576.96 nm and 579.07 nm

A spectrum of the signal being transmitted from the lamp was also collected. This was accomplished by faceting one end of the fiber cable in front of the lamp while plugged into the spectrometer. The fiber cable was mounted at a distance of less than 15 centimeters from the light source. This allows sample collection with effectively no interferences between the light source and point of detection. The lamp spectrum included in the fitting scenarios varied with the compound of interest being investigated. For NO_2 fits the lamp collected in the above described method was used. However, for NO_3 fits, a sample spectrum was chosen that was collected around either the sunrise or sunset. The lamp reference spectrum contains absorption features of the present gases excluding NO_3 since this gas is minimal during the daytime due to rapid photolysis. The lamp spectrum are used to account for all of the lamp features and used in equation 1.1 as $I_o(\lambda)$.

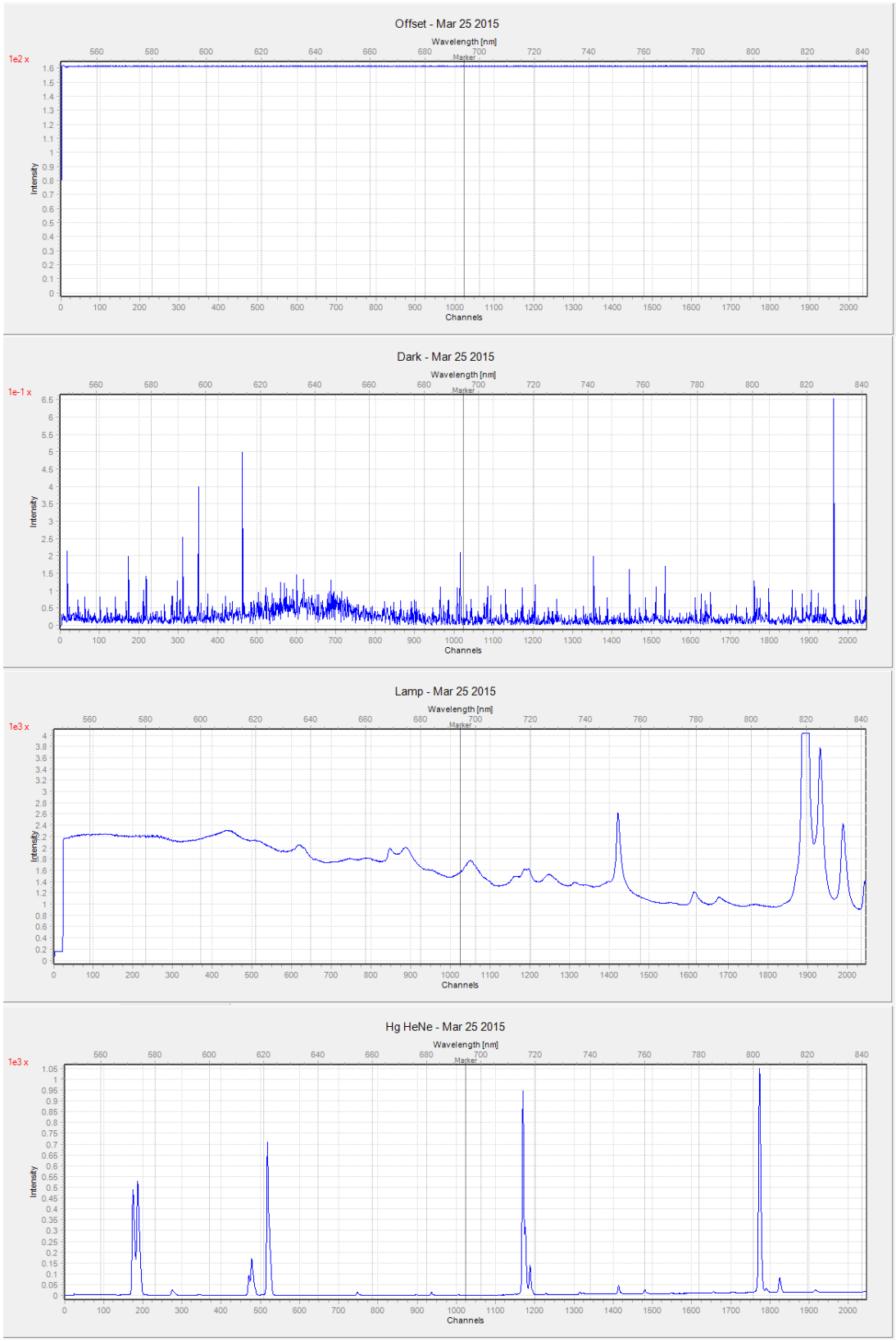

Figure 3: Sample calibration spectrum collected for Mar 25 2015. From top to bottom; Offset, Dark noise, Lamp and Hg HeNe

The data collected for all of these calibration spectra were then combined using specialized software, DOASIS, to create a fitting scenario. Each wavelength calibration must be applied to a spectrum before cross-sections of specific trace gases can be fit to a sample spectra. The mercury lamp and He-Ne laser spectra have their calibration applied to the sample spectra after the offset and dark noise are subtracted. The cross-sections used were obtained from various published sources (See Appendix A). These cross sections first have their wavelengths converted from vacuum to air conditions using a built-in function in the DOASIS software. They are convoluted using a convolution kernel into a blank spectrum which has been calibrated with the mercury/neon lamp data. This convolution acts to correct for the differences between the spectrometer used to collect the cross-sections and the spectrometer used to collect the sample spectra.

A fitting region is then chosen that ideally, contains distinct absorption features of the trace gas of interest. The fit ranges used for NO_2 and NO_3 were 560 – 585 nm and 617 – 672 nm, respectively. In order to analyze an entire night's data, a Jscript program was used to automate the fitting process. This script corrects and calibrates the measured spectra and fits the cross-sections to each spectrum iteratively. A sample of the script can be found in Appendix A.

2.3 Polynomial Fitting

The goal is then to combine all broadband features and separate them from the narrowband. This is accomplished using the software package DOASIS to fit a polynomial to the broadband features of a collected spectrum. The order of the polynomial is chosen based on the shape required, often 2^{nd} or 3^{rd}. This polynomial accounts for the broad band attenuation due to Rayleigh and Mie scattering. The polynomial also accounts for the broadband trace gas absorbance features and instrumental effects combining them into one variable, μ_m (Platt et al, 1979). The assumption is that the air mass and absorption remains constant along the path length and therefore is independent of path length. The equation becomes

$$\ln\left(I(\lambda, L) = \ln\left(I_o(\lambda)\right) - \left[\sum_{j=1}^{n} \sigma_j^i(\lambda, p, T) \times \int_0^L c_j(l)dl + \sum_{m=0}^{p} \mu_m \times \lambda^m\right]\right.$$

(E. 14)

This can be simplified to;

$$\ln\left(I(\lambda, L) = \ln\left(I_o(\lambda)\right) - \left[\sum_{j=1}^{n} \sigma_j^i(\lambda, p, T) \times S_j + \sum_{m=0}^{p} \mu_m \times \lambda^m\right]\right.$$

(E. 15)

The software then uses a method of least squares to find the values of S_j, slant column density, and μ_m that best reproduce the value of the measured signal $I(\lambda, L)$. The difference between the actual spectrum and the fit, χ^2, is then calculated. This minimum value can be found using a least square fit (Stuttz and Platt, 1996).

$$\chi^2 = \sum_{k=k_{\lambda 1}}^{k_{\lambda 2}} \left[\ln\left(I(k, L) - \ln\left(I_o(k)\right) + \sum_{j=1}^{n} \sigma_j'(k, p, T) \cdot S_j + \sum_{m=0}^{p} \mu_m' \cdot k^m\right]^2\right. \quad \text{(E. 16)}$$

This value is brought to a minimum through a least-square method (Albritton, 1976). For a successful retrieval you need all the absorption features of the traces gases that have strong differential features in the fitting range. The residual is effectively the difference between the measured spectrum and the modeled spectrum. A residual, R, will then remain which can be described by the following formula;

$$R(k) = l\ln\left(I(k, L) - \ln\left(I_o(k)\right) + \sum_{j=1}^{n} \sigma_j'(k, p, T) \cdot S_j + \sum_{m=0}^{p} \mu_m' \cdot k^m\right.$$

(E. 17)

The size of the residual can be used to indicate the quality of the fit. A stronger fit is one which has a lower residual value. Errors in the fit can arise due to failing to include the absorption cross section of a gas that is significantly absorbing. The software then applies shift and squeeze to find the best fit of the cross-section to the spectrum. These values are all then reported and used for the calculation of gas mixing ratios.

3. Results and Discussion

The measurements and analysis of NO_2 and NO_3 concentrations at York University between March 4 to March 8 and March 23 to March 26 will be presented and discussed. All measurements were made using Active-DOAS during a period just before sunset and until after sunrise. The results will be compared with the results from a TECO instrument to draw comparisons with. The success of fitting NO_2 in the fitting range of 560 - 585 nm will be discussed. In addition two case studies will be presented to highlight the differences in night time chemistry occurring during different environmental conditions.

3.1 NO_2 DOAS Fitting Procedure

The fitting procedure carried out follows the explained method in the Experimental section. The concentration of NO_2 was calculated using a fitting range of 560 - 585nm. The fitting range used previously for NO_2 has been 560 -585 nm however the fitting range was shortened to avoid a water feature. The fitting scenario for NO_2 included differential cross sections of NO_2 (Vandaele 1997), H_2O (Coheur, 2002) and O_4 (Hermans 1999). It also included the calibration data from the Hg lamp and He-Ne laser, offset and dark noise calibration and a 2^{nd} order polynomial fit to the broadband features of the spectrum. A sample NO_2 fit result from Mar 25, 2015 is shown with mixing ratio of 37.60 ± 0.88 ppb.

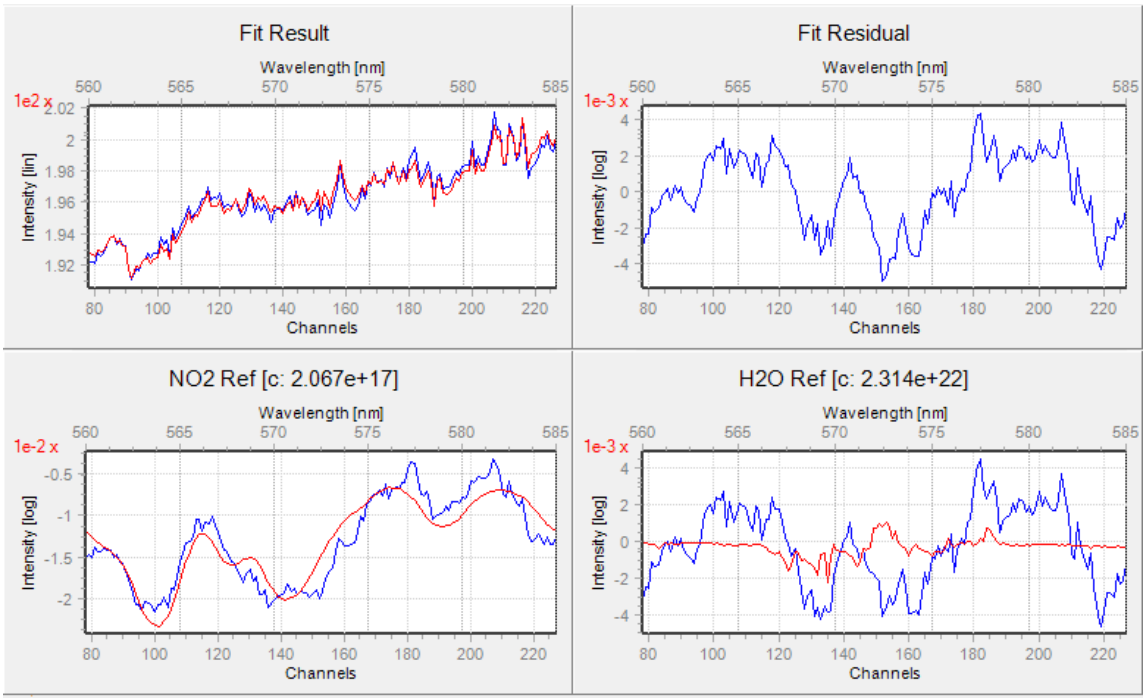

Figure 3.4: DOASIS fit result for NO_2 on Mar 25 2015 at 9:09pm. The mixing ratio obtained was 37.60 ± 0.88 ppb.

The values reported by the DOASIS software are a slant column density and associated error. These values must then be converted into a mixing ratio. This is accomplished by taking into account the path length and air mass temperature and pressure (See Appendix B). The error associated with each mixing ratio was calculated in a similar fashion.

3.2 NO_2 DOAS Fitting Results

The results from the analysis of NO_2 are summarized in table 3.1. The statistical summary displays the relative concentrations of the gases of interest as well as their distribution over the entire sampling time period.

	MAX	95%	75%	Average	Median	25%	Min	N
NO_3 (DOAS)								
NO_2 (DOAS)	58.01	39.59	27.50	19.41	16.03	11.10	< DL	2201
NO_2 (TECO)	56.00	40	29	20.76	19.00	12	3.00	9015
O_3 (TECO)	54.00	43	34	23.69	24.00	14	< DL	8863
NO (TECO)	0.00	21	5	4.53	1.00	1	< DL	9015
ΔT (^oC)	1.79	0.70	0.27	0.17	0.09	-0.08	-1.46	1428
WS (m/s)	7.82	4.93	3.18	2.49	2.21	1.58	0.31	1428

Table 3.1: Statistical summary of the observed NO_2 concentration at York University

Each of the two time periods which were sampled March 4 to 8 and March 23 to 26 displayed similar trends in values when tabulated separately. These values are summarized in Tables 3.2 and 3.3.

	MAX	95%	75%	Average	Median	25%	Min	N
NO_3 (DOAS)								
NO_2 (DOAS)	58.01	38.29	20.93	16.24	13.94	8.70	< DL	1131
NO_2 (TECO)	56.00	41	27	20.76	19.00	12	3.00	4682
O_3 (TECO)	54.00	45	39	28.23	32.00	18	< DL	4606
NO (TECO)	51.00	24	5	4.41	1.00	< DL	< DL	4682
ΔT (^oC)	1.79	0.96	0.34	0.15	0.10	-0.13	-1.38	699
WS (m/s)	7.82	5.44	3.79	2.85	2.61	1.83	0.52	699

Table 3.2: Statistical summary of the observed NO_2 concentration between March 4 and March 8 2015.

	MAX	95%	75%	Average	Median	25%	Min	N
NO_3 (DOAS)								
NO_2 (DOAS)	45.83	39.93	32.53	22.75	21.16	13.18	< DL	1070
NO_2 (TECO)	46.00	40	30	20.77	19.00	12	3.00	4333
O_3 (TECO)	42.00	34	27	18.78	19.00	10	0.00	4257
NO (TECO)	77.00	20	5	4.67	2.00	1	0.00	4333
ΔT (^oC)	0.87	0.55	0.23	0.09	0.09	-0.06	-1.46	729
WS (m/s)	5.62	4.02	2.57	2.13	1.94	1.47	0.31	729

Table 3.3: Statistical summary of the observed NO_2 concentration between March 23 and March 26 2015

In order to gain further insight into the night time chemistry occurring two case studies will be used. They will highlight the difference between stable and unstable atmospheric conditions. Both studies will make their measurements during time periods prior to sunset and ending after sunrise. This time frame was chosen to mimic the conditions for the long-term goal of simultaneous measurement of NO_2 and NO_3.

3.3 Case Study 1: Stable Night, March 5 2015

The night of March 5 2015 is categorized as a stable night based on its atmospheric conditions. [8] This is defined as a night with low winds and high ΔT. The average wind speed for the night was 1.58 m/sec while the maximum and minimums were 3.86m/s and 0.52m/s, respectively. A complete summary of the observed mixing ratios can be seen in Figure 4.2.

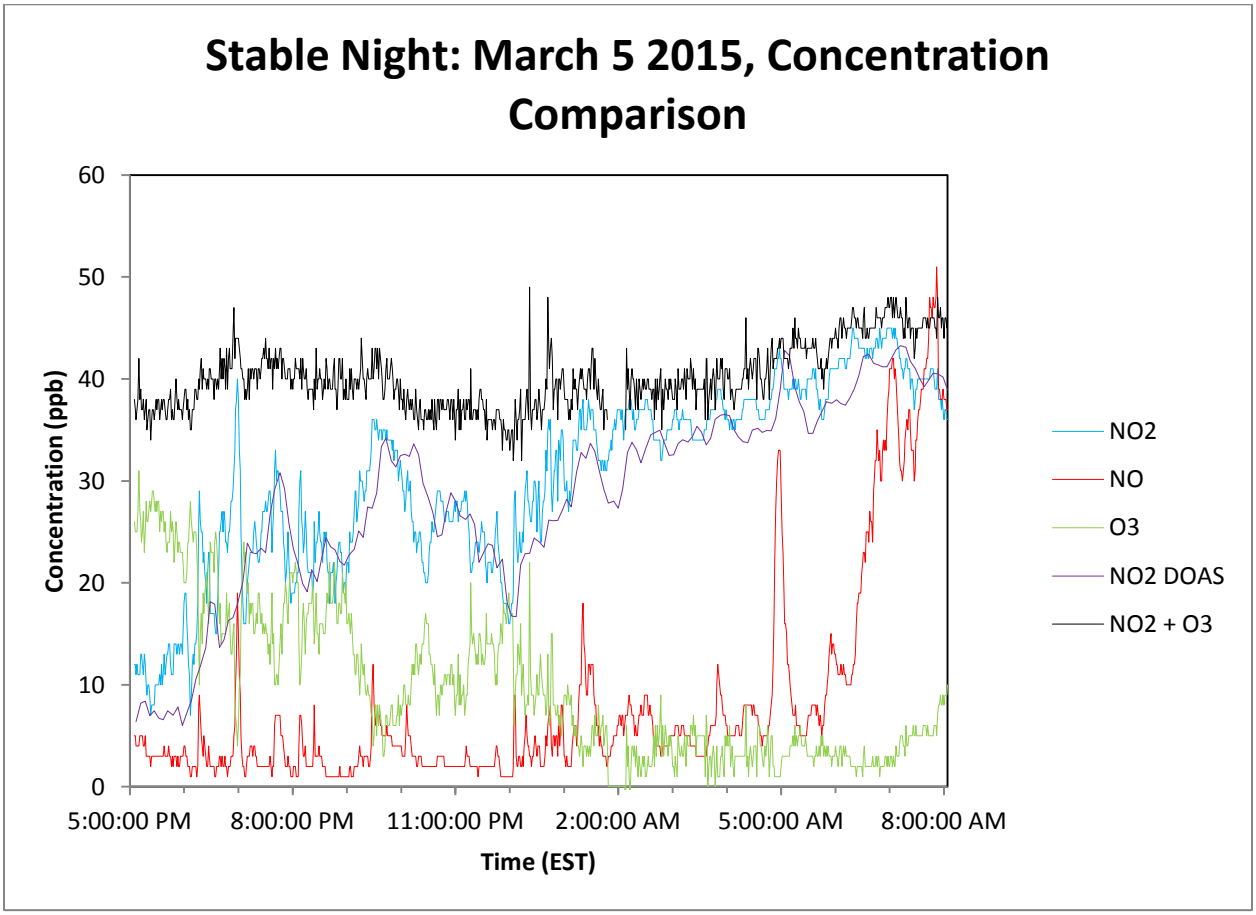

Figure 4.5: The overall gas concentration distribution for the night of March 5, 2015, displaying the comparison between the DOAS and TECO instrument measurements.

This figure gives a temporal representation in the change in concentrations over the night. From this graph three separate analysis will be presented to highlight the major trends observed; comparison of the DOAS and TECO NO_2 concentrations, anti-correlation between NO and O_3 and the presence or lack of NO_3 during periods containing NO. The comparison between the NO_2 concentrations observed by the DOAS and TECO instruments is done by plotting their

concentrations against each other. This was done by taking 4 minute averages of the TECO to allow for a direct comparison with the DOAS samples, which were measured on that time scale.

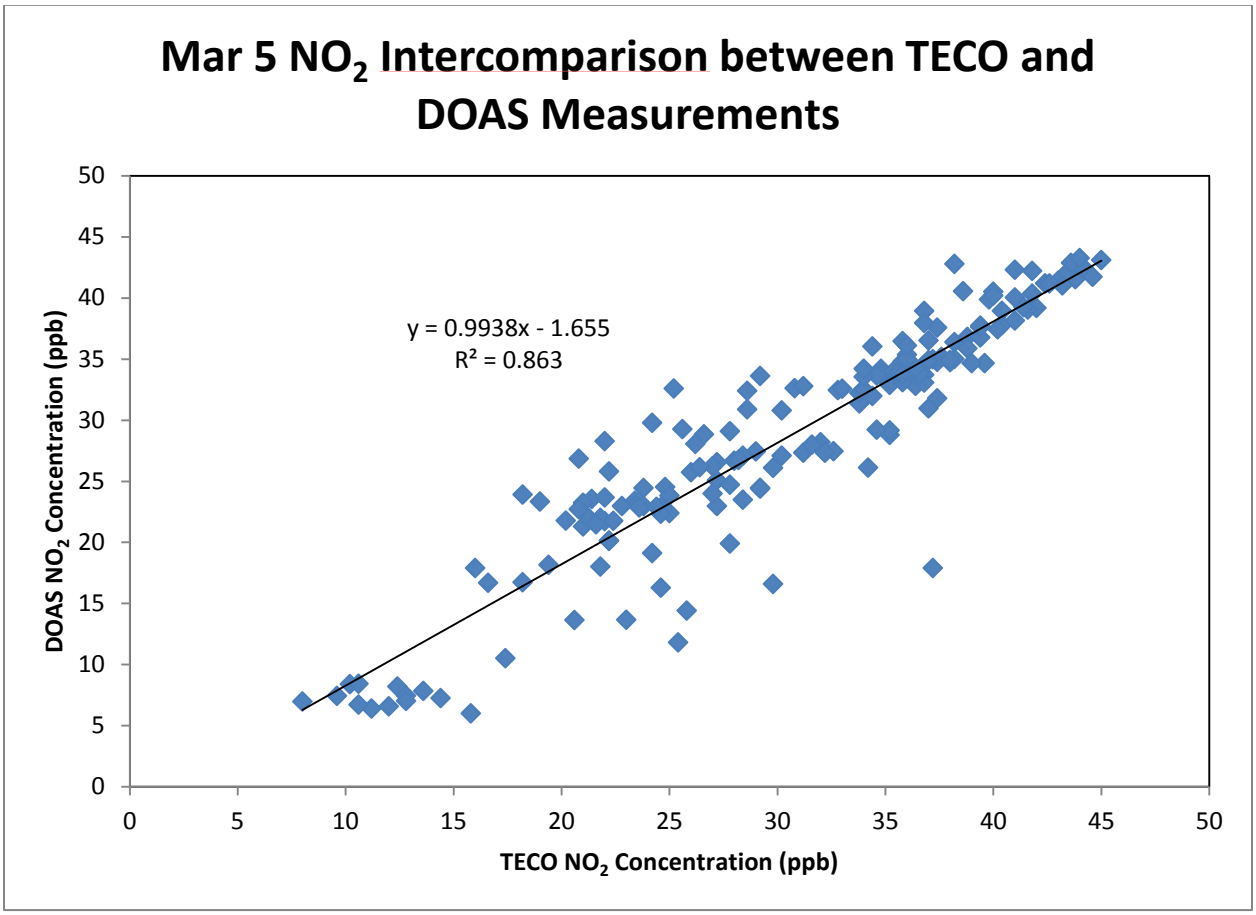

Figure 4.6: Comparison of the NO_2 concentration, in ppb, between the DOAS and TECO instruments. This graph shows the correlation between the two datasets to be linearly related. Equation: 0.99 ± 0.03 x – 1.66

This graph displays a strong intercomparison between the two instruments. The slope of the line is 1 within error which supports the methodology used to fit the NO_2 concentration using DOAS. This acts to validate this technique in determining the vertical column distribution of NO_2 and NO_3. Another point which can be drawn out from the gas profile from this night (Figure 4.2) is the horizontal line produced by odd-oxygen. The odd oxygen line is the sum of the O_3 and NO_2 concentrations. A relatively constant line occurs when the following reaction is taking place;

$$NO + 0_3 \rightarrow NO_2 + O_2 \qquad \text{(R. 11)}$$

This reaction shows that the increase in NO_2 concentration occurs at the same rate as the decrease in O_3 concentration. When the odd-oxygen line is horizontal and the concentrations of NO_2 and O_3 are anti-correlated reaction 4.1 is occurring.

The final point of note is the affect that the presence of NO will have on NO_3 formation. As highlighted in reaction 1.7 when NO is present at detectable levels it is expected that no NO_3 will be detected. This is due to the rapid reaction between NO_3 and NO to form two molecules of NO_2. With NO being detected on this night it is expected that NO_3 will not be found. The results of the NO_3 fit for this night are shown in Figure 4.4.

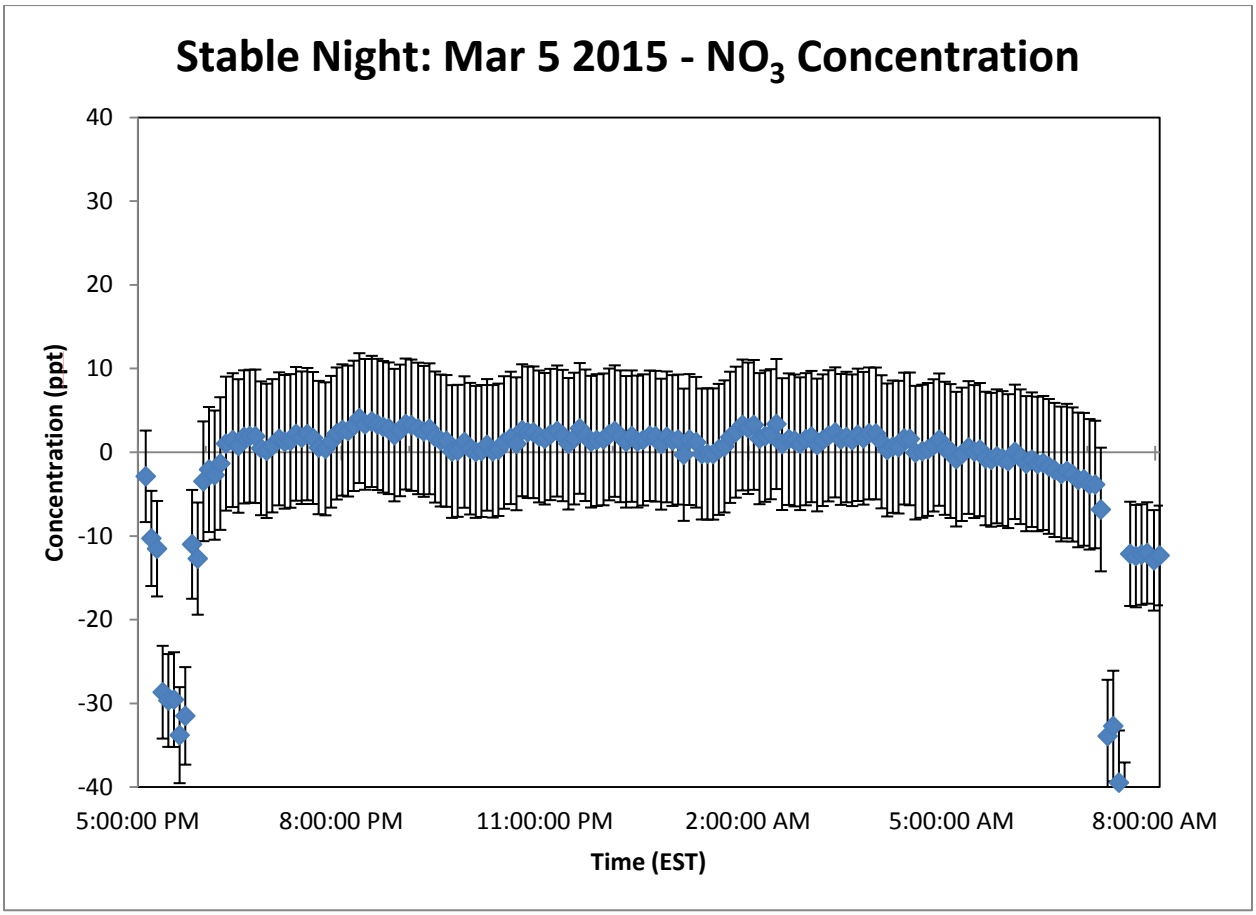

Figure 7.4: NO_3 concentration for the night of March 5 2015. Displays zero values due to presence of NO in the atmosphere.

The result of the NO_3 fit display a value of zero, within error, for the entire night. This has been shown to be as a result of the presence of NO in the atmosphere. The negative values in the graph occur at time periods around sunrise and sunset. They occur as a result of not

including solar features in the fitting scenario. Future fits could include these features to account for these values but they do not have an impact on the values except for periods near sunrise or sunset. Overall the results from this night agree with the previously explained atmospheric nitrogen chemistry. Also, the result from the intercomparison between the TECO and DOAS instruments supports the methodology used to fit NO_2 and NO_3.

3.4 Case Study 2: Unstable Night, March 8 2015

The night of March 8 2015 was labelled an unstable night based on its atmospheric conditions for the majority of the night. [8] This is defined as a night with high winds and low ΔT resulting in a large amount of vertical mixing of the air. However, towards the early morning the wind speed dropped and the ΔT value began to increase. The conditions of this case study toward its end are that of a stable night. The average wind speed for the unstable portion of the night was 3.08 m/sec and while the maximum and minimums were 5.54 m/s and 1.76 m/s, respectively. Comparisons between these distinct atmospheric conditions will be made to highlight the difference between the two case studies and within this night. A complete summary of the observed gas concentrations can be seen in Figure 4.5.

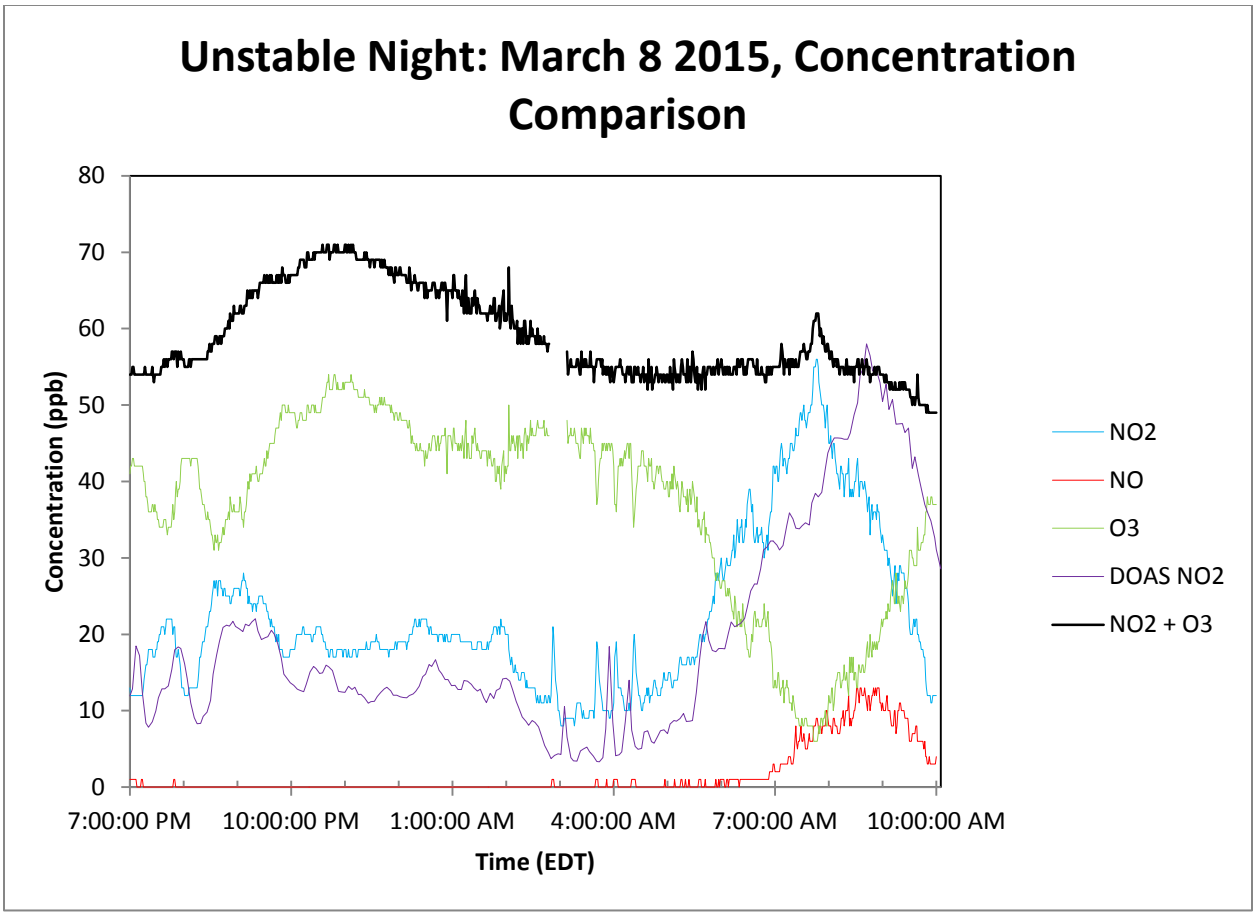

Figure 4.8: Displays the temporal gas concentrations of NO, O_3, odd-oxygen and NO_2 measured by the TECO and DOAS instruments.

The same three trends will be compared for this night as with March 5, 2015. The differences and similarities will be highlighted to demonstrate the impact that the atmospheric conditions have on the chemistry. The first comparison will then be the intercomparison between the concentration of NO_2 detected by the DOAS and TECO instruments.

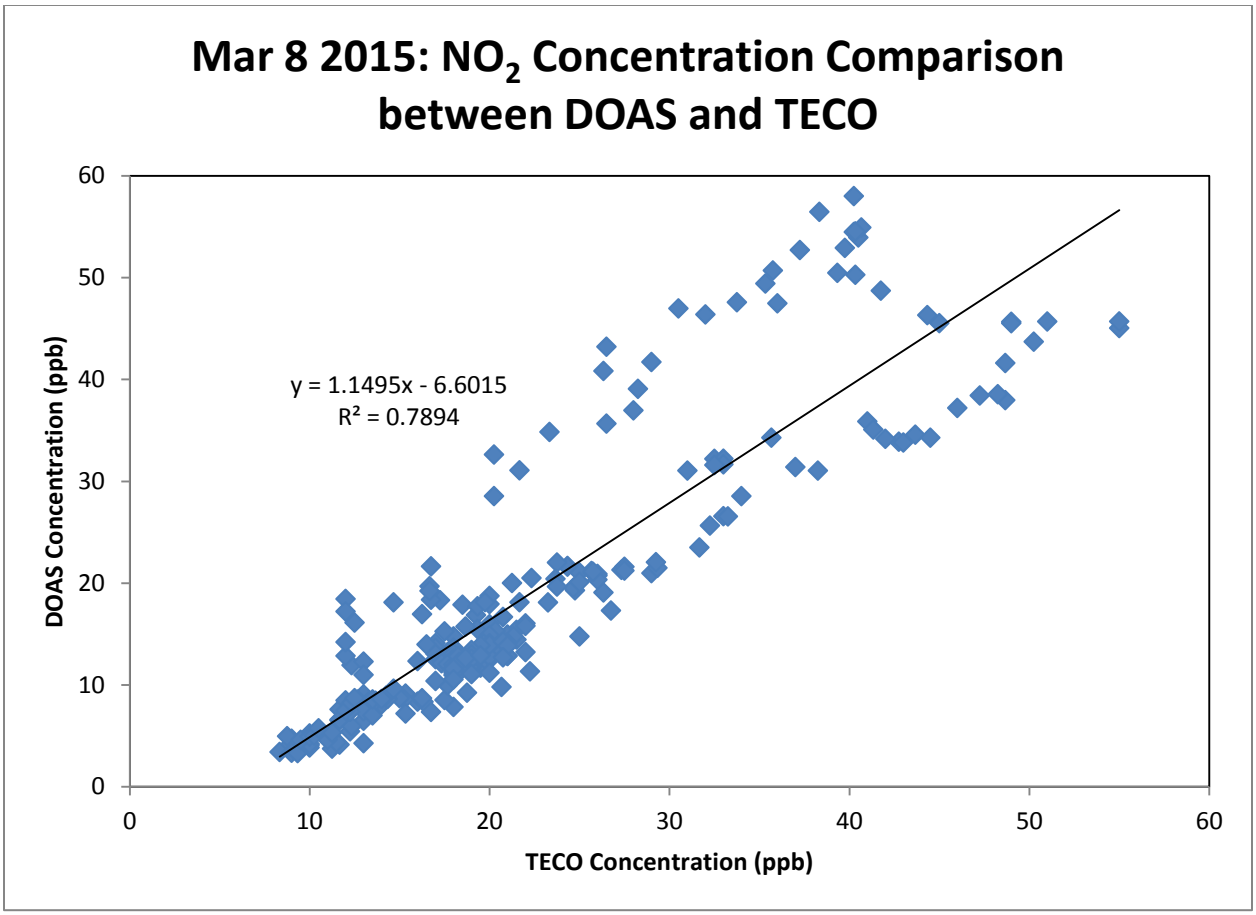

Figure 4.9: Comparison of the NO_2 concentration detected by DOAS and TECO instruments for the night of March 8 2015. Equation: 1.15 *± 0.04 x – 6.60*

Figure 4.6 represents the comparison between the DOAS and TECO instruments for the entire night of March 8 2015. The slope again is close to 1 with a strong agreement between the two data sets. When analyzing the comparison further it can be found that the majority of the points above the line of best fit are from after 7:30 pm, when the conditions changed from unstable to stable. This period of stable atmospheric conditions were categorized with an average wind speed of 1.58 m/sec and a ΔT of 0.51 ^{o}C. When the data points for the stable period of the night are removed the resulting comparison is affected, shown in Figure 4.7.

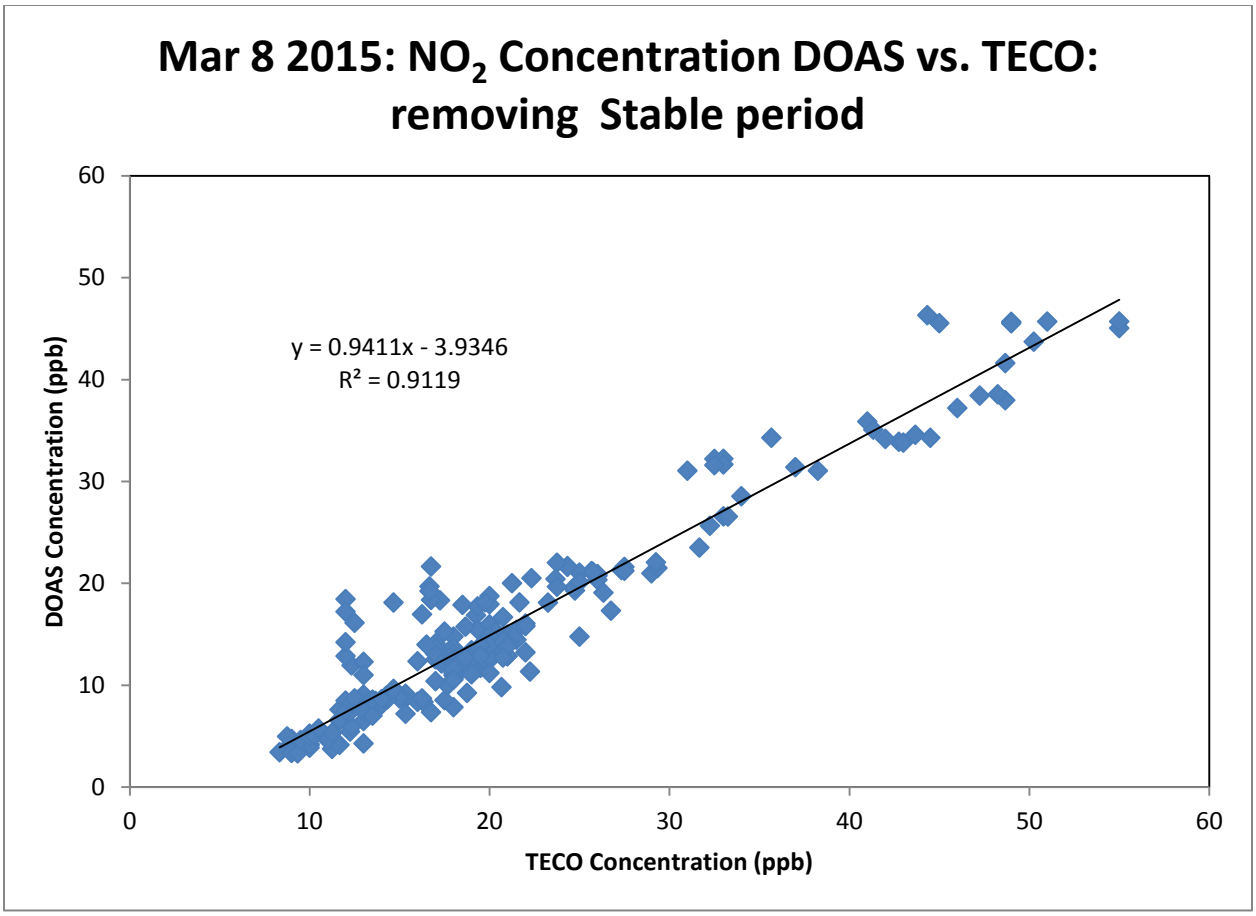

Figure 4.10: Comparison of NO_2 concentrations between the DOAS and TECO instruments. Only including data points during the period of unstable atmospheric conditions. Equation: 0.94 ±0.02 x – 3.93

Once again the slope of the line of best fit is close to 1 (0.94 ± 0.02) with a moderate agreement to the data. This demonstrates that different atmospheric conditions will affect the detection of the instruments. It also shows that the instruments show strong agreement in either unstable or stable conditions. This result leads to further support of the methodology used to fit NO_2 and NO_3 using DOAS. The observed peak of NO_2 and NO at 7:30 am correlates with rush-hour traffic. Due to York Universities close proximity to major roadways it was observed throughout this study that NO and NO_2 concentrations were elevated during peak traffic times.

The line of odd-oxygen once again demonstrates a constant value (Figure 4.5). The constant odd oxygen supports that reaction 4.1 is occurring to increase NO_2 concentration as O_3 concentration decreases. This point can be highlighted by analyzing the time period just before

and after 4:00am. During this time there are three distinct titration events with NO_2 displaying sharp peaks opposite to O_3 displaying sharp wells. The reaction at this time period is accompanied by a horizontal odd-oxygen line which demonstrates that the NO_2 and O_3 are reaction with each other.

The final comparison that can be made is the low concentration of NO throughout the night. As shown in reaction 7 if there is any NO present in the atmosphere it is expected to rapidly react with NO_3 to produce NO_2. This reaction will result in NO_3 concentrations being below detection limits. As a result of NO concentration being zero for the majority of the night it is expected that a detectable level of NO_3 may be able to form. The results of the NO_3 fit for this night are shown in Figure 4.8.

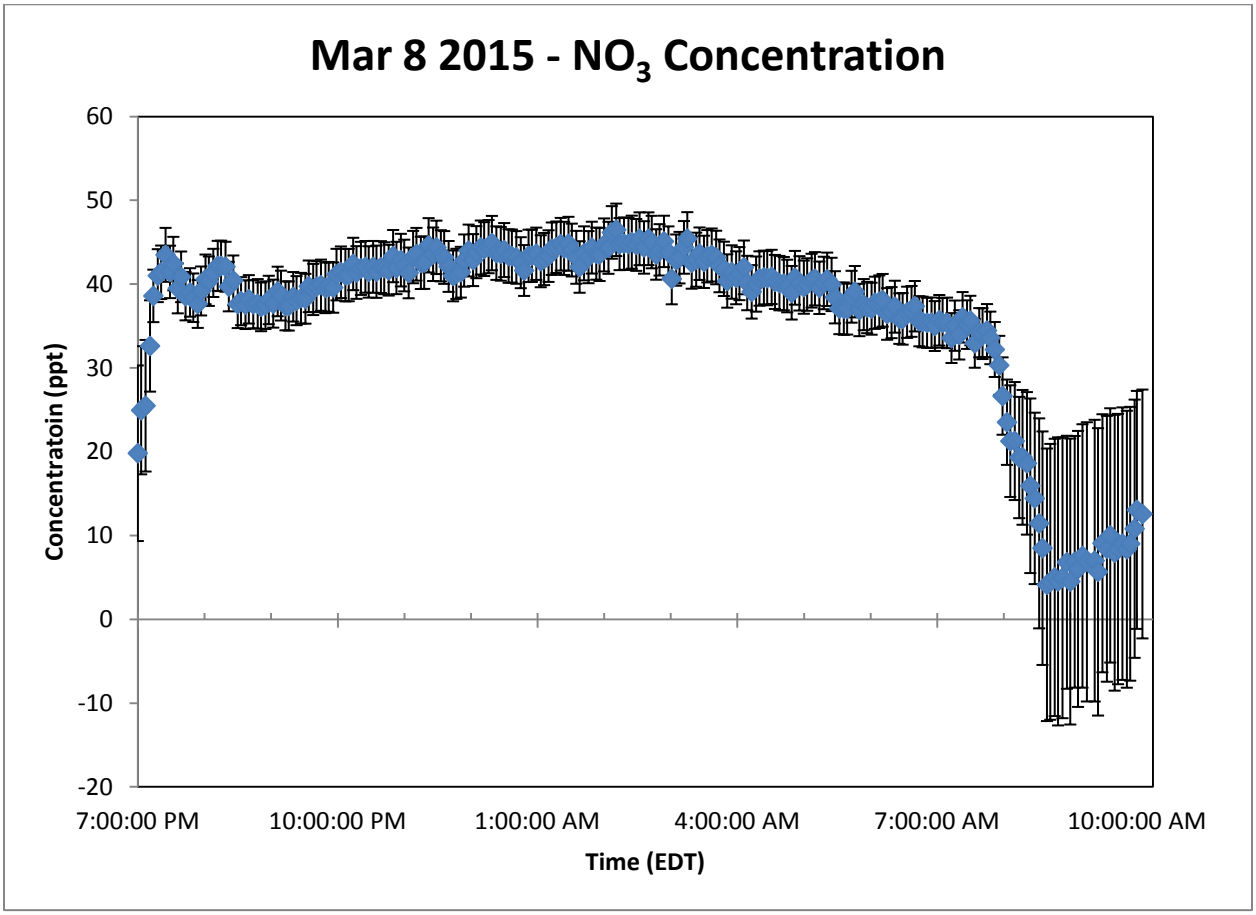

Figure 4.11: March 8 2015 NO_3 concentration

The concentration of NO_3 in Figure 4.8 demonstrates the build up of NO_3 concentration for the night of March 8 2015. This result is in agreement with the lack of NO present in the atmosphere. The concentration is relatively consistent throughout the night and then drops to zero in the morning. This drop in concentration is correlated both with sunrise and the rise in NO concentration, both of which have been demonstrated to reduce NO_3 concentration.

Now that NO_2 and NO_3 have been observed on the same night the calculation of N_2O_5 is possible. This is accomplished by using the reported equilibrium rate constant for reaction 1.9 (See Appendix C). The result of applying this calculation to the entire night is shown in Figure 4.9. N_2O_5 is an important molecule because it has been shown to be involved with two reactions which have significant impact on nitrogen chemistry. [10]

$$N_2O_5 + H_2O \rightarrow 2\,HNO_3 \qquad \text{(R. 12)}$$

$$N_2O_5 + Cl^- \rightarrow ClNO_2 + NO_3^- \qquad \text{(R. 13)}$$

These reactions demonstrate N_2O_5's ability to react with other species in the atmosphere to form molecules which will persist until morning. When exposed to sunlight the products of reactions 12 and 13 will undergo photolysis.

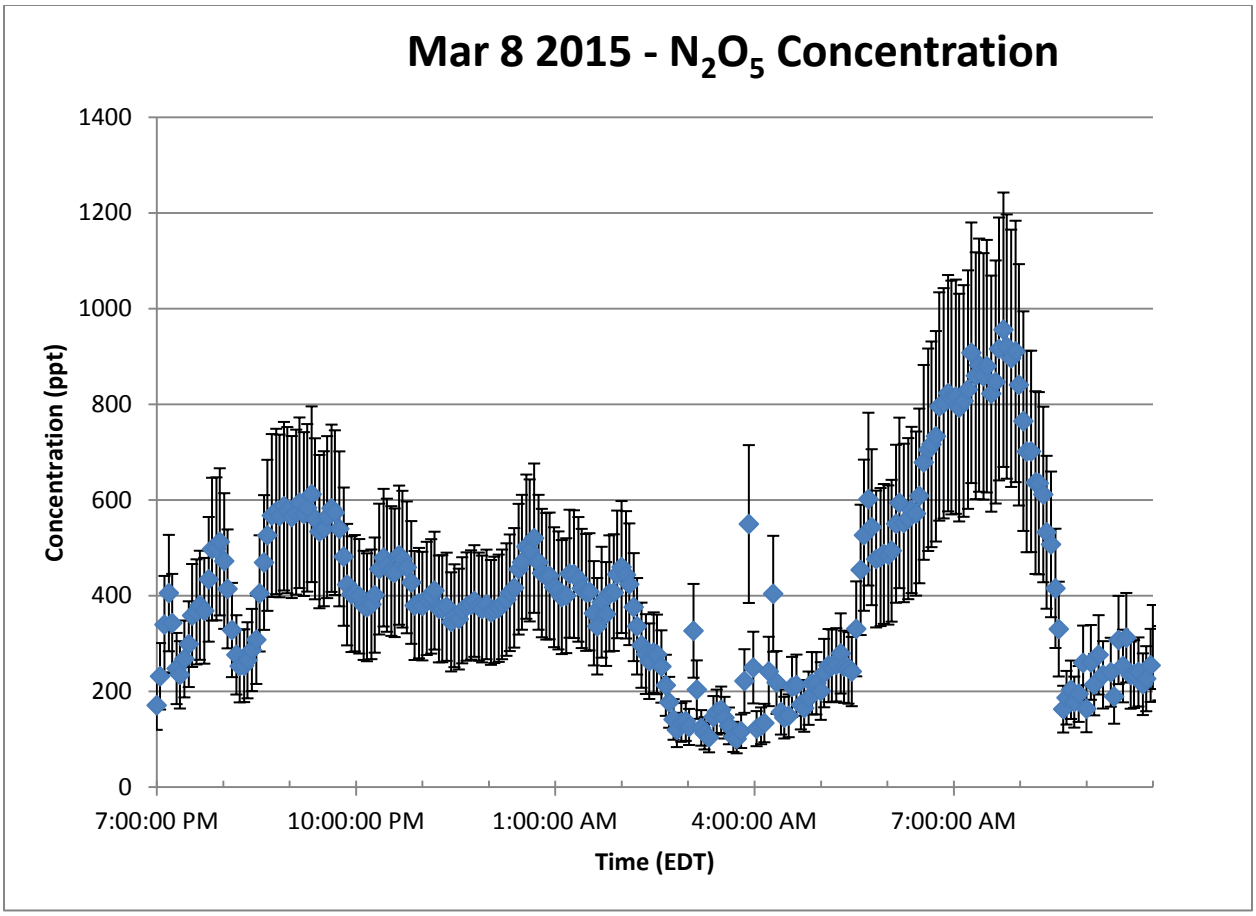

3.5 Summary of Results for Entire Data Set

In order to validate the methodology used to fit the NO_2 and NO_3 using DOAS a larger comparison was made with the TECO instrument (Table 4.4). As can be seen from these results the concentrations calculated from the DOAS instrument show a strong correlation with that of the TECO instrument. The notable deviations from strong correlation occur on March 7, 23, 24 and 26, 2015. The common factor between these nights is that that they are all on nights of either variable or stable atmospheric conditions. This demonstrates a stronger agreement between the instruments during unstable conditions. The difference between the two methods can be explained by the nature of both instruments. The DOAS instrument finds the average concentration over a fit path length while the TECO instrument takes measurements at a single point. The physical separation of these two techniques will inherently lead to differences between the resulting mixing ratios. The differences in the observed concentrations was

demonstrated to be stronger during periods of stable atmospheric conditions, when the air is not homogenously mixed.

Table 4.4; The slopes and R^2 values for the intercomparison of NO_2 concentration between DOAS and TECO instruments.

	Slope	Intercept	R^2	Conditions
March 4, 2015	1.01 ± 0.05	-4.43	0.75	Variable
March 5, 2015	0.99 ± 0.03	-1.66	0.86	Stable
March 6, 2015	1.03 ± 0.12	5.73	0.20	Variable
March 7, 2015	0.48 ± 0.04	6.01	0.42	Stable
March 8, 2015	1.15 ± 0.04	-6.60	0.79	Full-night
March 8, 2015	0.94 ± 0.02	-3.93	0.92	Removing stable
March 23, 2015	0.78 ± 0.03	7.67	0.71	Variable
March 24, 2015	0.68 ± 0.02	13.54	0.77	Variable
March 25, 2015	0.72 ± 0.07	5.09	0.68	Entire night
March 25, 2015	0.92 ± 0.03	3.03	0.89	Removing stable
March 26, 2015	0.69 ± 0.05	4.69	0.38	Variable

The atmospheric conditions were categorized based on their average meteorological data summarized in Appendix B. The nights were categorized based on their average wind speed and ΔT values. If the average wind speed was great than 5 m/s and the ΔT was less than $0.2^{o}C$ the night was labelled unstable. Conversely if the wind speed was lower than 2 m/s and the ΔT was greater than $0.5^{o}C$ the night was categorized as stable. [8]

4. Conclusions and Future Work

In this work Active-DOAS was used to analyze NO_2 and NO_3 concentrations in an urban environment t night. A new methodology was worked towards for simultaneously fitting NO_2 and NO_3 in the red portion of the S2000 Ocean Optics Spectrometer was established. One case study was shown how the simultaneous measurements of NO_2 and NO_3 can be used to determine the concentration of N_2O_5. Using the equilibrium rate constant of the reaction $NO_3 + NO_2 \rightleftharpoons N_2O_5$ the concentration of N_2O_5 was calculated. Two case studies were used to display the impact of differing atmospheric conditions.

Appendix

A. Differential Cross-Sections Used;

Yokelson, 1994	NO_3
Vandaele, 1997	NO_2
Coheur, 2002	H_2O
Hermans, 1999	O_4

B. Conversion of signal from DOASIS into a concentration: is accomplished by first dividing the slant column density from DOASIS by the path length;

$$\frac{2.067\ \times 10^{17} molecule \cdot cm^2}{216\ 000\ cm} = 9.571 \times 10^{11}\ molecule \cdot cm^3$$

This value is then corrected for the air mass factor by division;

$$\frac{9.571 \times 10^{11}\ molecule \cdot cm^3}{2.49\ \times 10^{19}\ molecule \cdot cm^3} = 3.843 \times 10^{-8}$$

This value is then converted into a concentration by multiplying by a factor appropriate to the desired concentration;

$$3.843 \times 10^{-8} \times 10^{9}\ ppb = 38.43\ ppb$$

C. Calculation of N_2O_5: began by converting the slant column density of both NO_2 and NO_3 into the same units as the rate constant. The sample calculation is shown for NO_3;

$$\frac{1.0652\ \times 10^{14} molecule \cdot cm^2}{216\ 000\ cm} = 4.931 \times 10^{8}\ molecule \cdot cm^3$$

This value is then used with the equilibrium rate constant and NO_3 concentration to determine the concentration of N_2O_5;

$$[N_2O_5] = k[NO_2][NO_3]$$

$$[N_2O_5] = (2.9 \times 10^{-11} cm^3 molecule^{-1})(4.931 \times 10^8\ molecule\ cm^3)(4.931 \times 10^{10}\ molecule\ cm^3)$$

$$[N_2O_5] = 4.26 \times 10^9 molecule\ cm^3$$

This value must then undergo the same calculation to be converted into a concentration, starting with the correction for air mass factor;

$$\frac{4.26 \times 10^9 molecule\ cm^3}{2.49\ \times 10^{19}\ molecule \cdot cm^3} = 1.711 \times 10^{-11}$$

This value is then converted to parts per trillion;

$$1.711 \times 10^{-8} \times 10^{12}\ ppb = 171.1\ ppt$$

References

1. Dr. S. Sanz Fernández de Córdoba (2004-06-24). "The 100 km Boundary for Astronautics". Fédération Aéronautique Internationale.

2. Lenner M. Nitrogen dioxide in exhaust emissions from motor vehicles. Atmospheric Environment. 21 37-43. 1987

3. Platt U, Perner D and Patz H. Simultaneous measurements of atmospheric CH_2O, O_3 and NO_2 by differential optical absorption. 1979. J of Geophysical Research. 84.

4. Wängberg I, Etzkorn T, Barnes I, Platt U and Becker K. Absolute determination of the temperature behavior of the $NO_2 + NO_3 + (M) \leftrightarrow N_2O_5 + (M)$ equilibrium. The Journal of Physical Chemistry A, 101, 9694 – 9698. 1997

5. Stutz J and Platt U. Numberical analysis and estimation of the statistical error of differential optical absorption spectroscopy measurements with least-squares method. Appl. Optics, 35, 6041-6053, 1996

6. Albritton D, Schmeltekopf A and Zare R. Moleculare Spectroscopy: Modern Research. Orlando, Florida, USA: Academic Press, 1976.

7. Wayne R, Barnes I, Biggs P, Burrows J, Canosa-Mas C, Hjorth J, Bras GL, Moortgat G, Perner D, Poulet G, Restelli G and Sidebottom H. The nitrate radical: Physics, chemistry, and the atmosphere, Atmospheric Environment. Part A. General Topics. 25, (1). 1991.

8. Wojtal Thesis, York University, 2013.

9. Finlayson-Pitts B and Pitts Jr. J. Chemistry of the upper and lower atmosphere. 2000. Academic Press, New York.

10. Dentener F and Crutzen P. Reaction of N_2O_5 on Tropospheric aerosols: Impact on the Global Distributions of NO_x, O_3 and OH. Journal of Geophysical Research. (98) 7149 – 7163. 1993